

Repulsive Osmotic Delamination: 1D Dissolution of 2D Materials

Volodymyr Dudko, Olena Khoruzhenko, Sebastian Weiß, Matthias Daab, Patrick Loch, Wilhelm Schwieger,* and Josef Breu*

2D materials have proved their potential in nearly every area of material science and chemistry. Unfortunately, large-scale production of nanosheets is not straightforward. Current methods suffer from low yield, uncontrollable defects, and requires a high-energy input. There is always a tradeoff between high quality and high yield. In this review, the alternative is highlighted to existing methods of 2D nanosheet production – 1D dissolution, historically known as osmotic swelling. As a thermodynamically driven, and therefore spontaneous, process it provides numerous benefits such as high aspect ratio and defect-free nanosheets with a quantitative yield. In this review, the theory behind this process is discussed, compare it with the existing methods, and highlight the key features that allow to extend 1D dissolution to different charged layered materials. Moreover, the applications in which nanosheets obtained by 1D dissolution proved to be advantageous due to their unique, processing-related features are discussed.

of stacked nanosheets (tactoids), where the diameter of the nanosheet stacks may easily be in the range of hundreds of nanometers to micrometers wide, while the thickness of individual nanosheets is only a couple of nanometers.^[4] This anisotropy of the individual nanosheets results in an enormous surface-to-volume ratio^[5] and a pronounced directional dependency of properties such as moduli.^[6]

Almost 20 years have passed since the groundbreaking work of Novoselov and Geim on the extraordinary properties of monolayer graphene that sparked a broad interest for 2D materials.^[7] By now, hundreds of 2D materials have been isolated and studied.^[8] 2D materials have found an application in catalysis,^[3,9] electronics,^[10] sensors,^[11] the biomedical field,^[12] and

others.^[13] Yet, an effective and universal approach to delaminate and produce 2D materials with monodisperse thickness on large or even industrial scale is still lacking.

The full story of delaminated materials starts much earlier in science history. The first 2D materials known to humanity were most likely clay and what is now called graphene oxide.^[14] Upon immersion into water,^[14a,15] selected clay minerals could disperse homogeneously, forming a viscous suspension consisting of nanometer-thick clay sheets. The roots of this phenomenon were thoroughly studied in the 1960s where the phenomenon was labeled “osmotic swelling.”^[14a,16] While this historic term suggests that the process is related to osmotic pressure, we will show that the initial phases of repulsive osmotic delamination rather have to do with the dissolution of ionic crystals. By means of the reported repulsive osmotic swelling, clay tactoids separate into individual single-layer nanosheets at distances of hundreds of nanometers.^[17] The process is spontaneous,^[17–18] thus requiring no additional energy input to completely delaminate the pristine layered material. Osmotic swelling allow maximizing the yield, obtaining the nanosheets with the strictly monolayer thickness and unique mesophase with the liquid crystalline state of the nanosheets. If only every 2D material could be prepared similarly!

Several reviews have focused on shear force driven liquid phase exfoliation of various 2D materials^[19] and therefore we disregard this process in this review. Liquid phase exfoliation may currently be regarded the state of the art process for exfoliation despite its reliance on brute force procedures like high-power ultrasonication. In this review, we will rather strictly focus on purely thermodynamically driven and therefore


1. Introduction

Material properties on the nanoscale can be different from the bulk. For instance, bulk gold is a shiny yellow metal, while gold nanoparticles can have a range of colors from wine red to deep blue depending on the shape and size.^[1] Materials that are inert in the bulk form become catalytically active at the nanoscale^[2] due to the electronic structure being modulated by quantum size effects. Most of these fascinating properties have roots in quantum and surface phenomena.^[3]

For 2D materials, additional unique properties arise from extreme anisotropy. Layered materials usually come in the form

V. Dudko, O. Khoruzhenko, S. Weiß, M. Daab, P. Loch, J. Breu
Bavarian Center for Battery Technology
Bavarian Polymer Institute and Department of Chemistry
University of Bayreuth
Universitätsstr. 30, 95440 Bayreuth, Germany
E-mail: josef.breu@uni-bayreuth.de

W. Schwieger
Institute of Chemical Reaction Engineering
Friedrich-Alexander-Universität Erlangen-Nürnberg
Egerlandstrasse 3, 91058 Erlangen, Germany
E-mail: wilhelm.schwieger@fau.de

 The ORCID identification number(s) for the author(s) of this article can be found under <https://doi.org/10.1002/admt.202200553>.

© 2022 The Authors. Advanced Materials Technologies published by Wiley-VCH GmbH. This is an open access article under the terms of the Creative Commons Attribution License, which permits use, distribution and reproduction in any medium, provided the original work is properly cited.

DOI: 10.1002/admt.202200553

spontaneous delamination processes that consequently require no input of shear force at all. These unfortunately are currently regarded a niche process mainly known in the lay science community. Historically it was referred to by “osmotic swelling.” As we elaborate on later this process, however, in its initial steps has nothing to do with osmotic pressure but rather resembles dissolution of ionic solids in solvents. For layered ionic materials, the dissolution obviously is limited to the stacking direction of the nanosheets and therefore we suggest labeling it 1D dissolution. Calling it differently from liquid phase exfoliation hopefully will help on the long run to clearly realize the fundamental differences between the two protocols to manufacture nanosheets. We will stress the key features of the osmotic swelling process rendering it a rather broadly applicable delamination method. Moreover, we will highlight some applications that are enabled by the unique features of osmotically swollen nanosheet suspensions.

2. 1D Dissolution

2.1. Mechanism and Driving Forces

The distinct feature of 2D materials is the inherent anisotropy of chemical bonding. In two dimensions, it possesses strong, partially covalent bonding. In order to build a layered crystal, there are weaker, yet still cohesive, noncovalent interactions in the third (stacking) direction, yielding stacks of nanosheets (Figure 1). In van der Waals crystals, the cohesive interactions are considerably weaker^[20] than those in ionic layered solids that are held together by Coulomb attraction (Figure 1).^[21] This Coulombic attraction can, however, be reversed to repulsion, which is the essence of osmotic swelling and 1D dissolution.

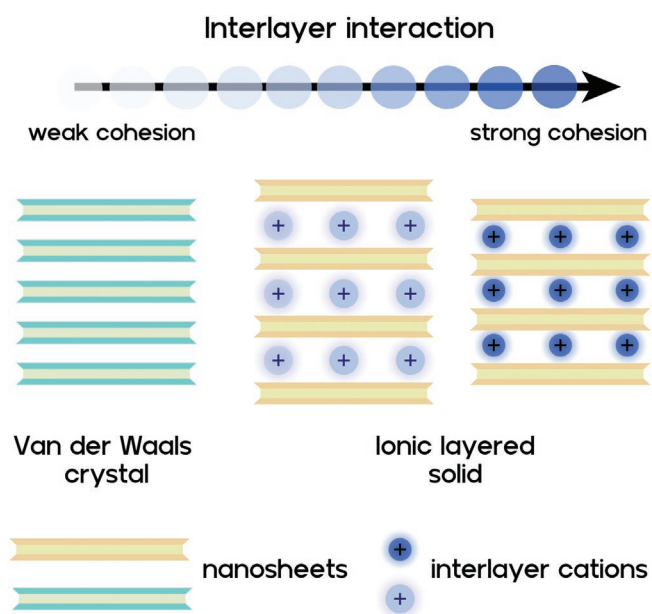


Figure 1. Types of layered compounds and relative strength of cohesive interactions holding together the nanosheets in the stack.

Due to the weak interactions in the stacking direction of layered materials, they can be modified by soft, intracrystalline reactions that are topotactic in nature, meaning that the periodicity in the stacking direction is changed (d-spacing or basal spacing), while the 2D structure of the nanosheets remains unaltered (Table 1). For instance, with anionic layers that are of focus here, upon ion exchange with bulky cations, their d-spacing increases and thus weakens the cohesive interaction. Alternatively, by solvation of interlayer ions, which is referred to as crystalline swelling, the d-spacing may also be enlarged and the shear lability may consequently be increased.^[22]

Contrary to osmotic swelling, crystalline swelling refers to a distinct phase transition with defined stoichiometry. As a function of the type of interlayer ion and the activity of the swelling agent (e.g., water vapor defined by relative humidity), solvent is incorporated into the interlayer space in discrete steps (e.g., one-, two-, or three-layer hydrate in hectorites).^[23] Swelling and de-swelling in the crystalline swelling regime is connected to a hysteresis as expected for a first order phase transition.^[23] If the basal surfaces carry functional groups, for instance silanol groups as with zeolites, molecules might be covalently, and therefore irreversibly, attached. Such grafting reactions also force an increase of the d-spacing (Table 1).

Most importantly, as long as the individual nanosheets in the layered crystal are cohesively stacked, the top-down process applied to obtain exfoliated materials requires energy input as thermodynamically required. The state-of-the-art and well-established way of exfoliating such cohesively stacked layered crystals is the so-called liquid phase exfoliation^[21] where (strong) shear forces exerted on suspensions are capable of thinning the pristine stacks all the way down to individual nanosheets.^[24]

Please note that while the separation of stacks into nanosheets is referred to in the literature as exfoliation or delamination, often as interchangeable synonyms, here we strictly follow the definition proposed by Gardolinski and Lagaly^[25] for clay minerals: “Exfoliation is defined as the decomposition of large aggregates (booklets) into smaller particles; delamination denotes the process of separation of the individual layers of the particles.” In this line, liquid phase exfoliation should be regarded as incapable of achieving delamination.

General terminology relating to 2D materials is diverse within the field, as several different scientific communities with distinct backgrounds, ranging from silicate chemists, colloidal chemists, mineralogists, zeolite chemists, physicists, crystallographers, and theoreticians take an interest in these materials. Everyone uses different terminology to refer to layered compounds and nanosheets derived thereof. In order to clarify the terminology, we propose the following terms in order to establish a common ground:

- Tactoid: a stack of layers; since individual layers are stacked with frequent faults or even in a completely random way, these stacks of layers lack a strict crystallographic phase relationships and consequently should not be referred to as crystals, but as tactoids.
- Intercalation: Incorporation of atoms, ions, or molecules into a layered host structure. It is a topotactic reaction with the 2D structure where the layers remain essentially unchanged, while the inserted material is present between the layers.

Table 1. Topotactic intracrystalline reactions (e.g., intercalation, e.g., grafting, ion-exchange, swelling) that increase the basal spacing and thus decrease the cohesive energy in the stack.

Type of reaction	Grafting	Ion-exchange	Swelling	
			Crystalline	1D dissolution
Reversibility	Irreversible	Reversible	Reversible	Reversible
Bonding type	Covalent	Ionic interaction, noncovalent	Stepwise noncovalent	Quasicontinuous noncovalent
Type of interactions of adjacent nanosheets	Cohesive	Cohesive	Cohesive	Repulsive

Intercalation commonly involves ion exchange or solvation reactions.

- Interlayer refers to the region between the two adjacent layers in a tactoid.
- (Intracrystalline) swelling involves an increase in the basal spacing of a layered compound to accommodate H₂O or other solvent or gaseous molecules within the interlayer.
- Exfoliation: slicing of tactoids into thinner stacks with multimodal thickness distributions
- Delamination: exfoliation of a layered material to the level of individual, single-layer nanosheets; a state in which translational symmetry along the stacking direction is completely destroyed.

Most commonly, the excess energy required to overcome cohesion forces is provided by high power ultrasonication (First line **Table 2**). This brute force method mechanically break weak van der Waals bonds but does not provide control over the thickness distribution of the resulting materials. Liquid phase exfoliation produces dispersions of 2D materials consisting of single, double, and multilayer nanosheets.^[8b,21,26] It is also energy-intensive, difficult to scale,^[27] and often offers only a modest yield of nanosheets. Needless to say, the excess energy requirement also causes breaking of the nanosheets, yielding aspect ratios far from the potential maximum given by the inherent diameter of the pristine layered material.^[28] Moreover, collapse of the cavities produced by ultrasonication produces very high local temperatures and potentially produces radicals that might be capable of chemically modifying the surface of the nanosheets produced this way.^[29]

Contrary to this, a handful of ionic-layered compounds show the long-known^[33] but rare phenomenon of so-called osmotic swelling. For this class of materials like layered transition metal oxides, layered antimony phosphates, graphene oxide, layered zeolites, or smectites, and thermodynamically driven (i.e., spontaneous) method for delamination exists: repulsive osmotic swelling, or more appropriately called “one-dimensional dissolution” (1D dissolution). This is a thermodynamically allowed process based on repulsive interactions between charged nanosheets. It produces a complete delamination with 100% yield and forms colloidal stable suspensions consisting only of individual nanosheets. Moreover, the gentle nature of this process allows preservation of the aspect ratio inherent to the starting material and does not introduce additional defects into the nanosheet structure (fourth line **Table 2**). Comparison of common exfoliation method and 1D dissolution are given in **Table 2**.

In this line, delamination by osmotic swelling resembles the dissolution of salts (**Figure 2a**). When an ionic crystal like sodium chloride is immersed into water, we are not surprised when it starts to dissolve. Water molecules solvate ionic constituents at the surface and separate them into solvated ions (**Figure 2b**). Strong electrostatic attraction between positively and negatively charged ions must be overcome by the interaction with the solvent molecules (**Figure 2c**). Dissolution is partially driven by the enthalpy of solvation. Additionally, the entropy increases during the dissolution process and may allow for the dissolving of crystals even with endothermic enthalpy of dissolution. Overall, dissolution is a thermodynamically driven process (exergonic) with all enthalpic and entropic contributions involved overriding the lattice energy.

Table 2. Comparison of advantages and disadvantages of different exfoliation methods and 1D dissolution.

Exfoliation method	Type of materials accessible ^{a)}	Advantages	Disadvantages
Mechanical ^[26b,27,30]	2 D van der Waals crystals like graphene, boron nitride, black phosphorous, metal dichalcogenides	Suitable for most 2D materials, simple equipment, easy to use, universal	Low yield, high energy input, low aspect ratio, defects and functional groups may be introduced, broad thickness distribution
Hydrothermal ^[31]	Materials that show crystalline swelling, potentially after redox-modification rendering the materials more shear labile: metal dichalcogenides, metal hydroxides, metal oxides, MXenes	Moderate yield, narrow lateral size distribution	Defects may be introduced, requires special equipment, nonuniversal.
Electrochemical ^[32]	As above, crystalline swelling is, however, triggered by redox modification by an external field: graphene, black phosphorous, metal dichalcogenides, MXenes, metal oxides	High yield, narrow thickness distribution.	2D materials must be electrically conductive, requires high quality crystals, requires electrochemical equipment
1D dissolution	Silicates, zeolites perovskites, acids. oxides	Strictly monolayers, quantitative yield, direct formation of electrostatically stabilised liquid crystalline phase, no surfactants required	Limited to ionic layered solids, requires special protocol for every material, nonuniversal.

^{a)}All materials referred here are of layered morphology

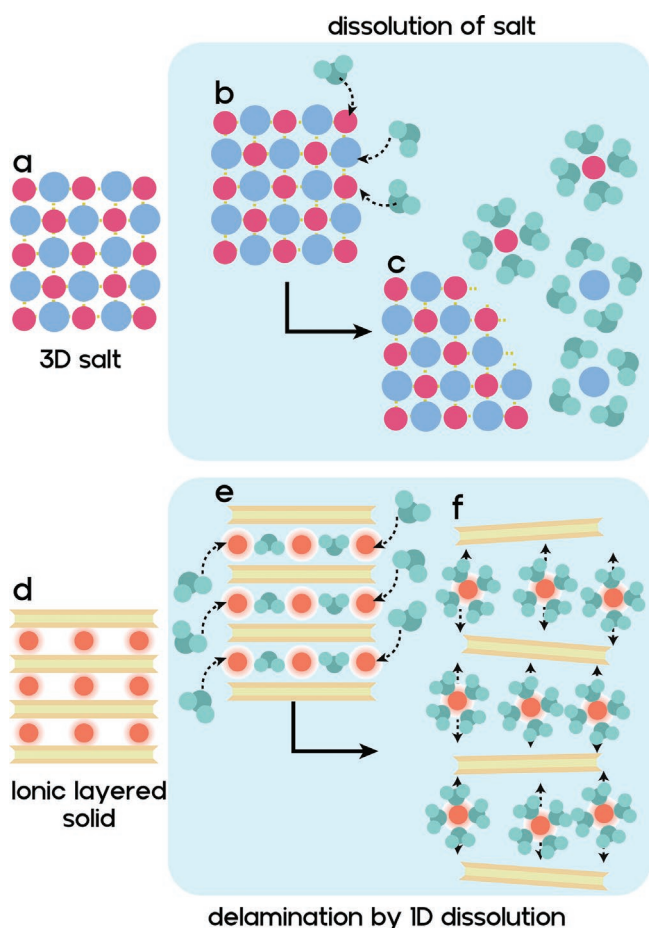


Figure 2. Schematic of the dissolution of a 3D crystalline salt and the 1D dissolution of a layered material. Crystalline salt. a) Upon immersion in water it starts to readily dissolve. b) Until complete dissolution with formation of c). A homogeneous solution of ions. Ionic layered solid. d) Upon immersion into solvent, solvent molecules start to solvate the interlayer ions e) and upon reaching of the critical threshold separation 1D dissolution into a nematic liquid crystalline suspension takes place f).

Repulsive osmotic swelling is a fundamentally similar process to the dissolution of salts, but limited to 1D due to the layered compounds' anisotropic nature (Figure 2d). In order to be spontaneous, the solvent has to overcome the adhesive interaction between the interlayer ions and charged nanosheets. At low activity, solvent molecules initially solvate the interlayer ions in discrete steps (Figure 2e) and increase the separation distance of nanosheets. To demonstrate the essential ingredients of 1D dissolution, we will focus on the swelling of 2:1 layered silicates (clay minerals) with water in the following. The initial swelling of clay minerals occurs in discrete steps and is referred to as crystalline swelling, as previously mentioned (Figure 2e and Figure 3).^[16e] Once the clay tactoids are immersed into water, the activity of the swelling agent is thus greatly increased, and the uptake of solvent molecules might continue beyond the limits of crystalline swelling. If this increases beyond a critical threshold of separation, the interaction between adjacent nanosheets in the stack is no longer attractive but rather becomes repulsive. The nanosheets separate themselves to equal distances (Figure 2f) much larger than

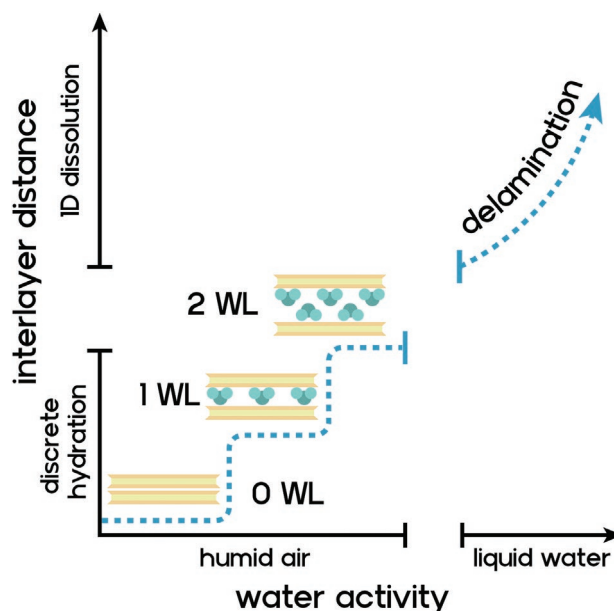


Figure 3. Schematic illustration of the transition of crystalline swelling to delamination via 1D dissolution as a function of water activity.

what is found in the crystalline swelling regime (Figure 3). For 1D dissolution to be triggered, the interlayer cations must leave the symmetrical position in the middle of the interlayer space and segregate into the Helmholtz-layers belonging to one of the two adjacent clay layers formerly circumscribing the interlayer space. This process requires monovalent interlayer ions and is fostered by the translational entropy contribution of interlayer species (ions and solvent molecules). As a result, overlapping diffuse double layers electrostatically repel adjacent clay layers in the stack (Figure 4).^[17] The separation of nanosheets at this point is h/Φ , where h is the thickness of individual nanosheets and Φ the volume content of clay in the aqueous suspension.

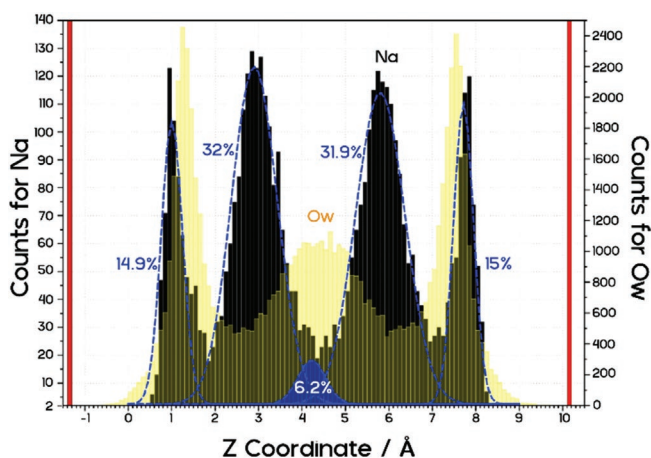


Figure 4. Histogram of the z-distribution of Na^+ (black bars) and water molecules ("Ow", yellow bars) in the interlayer space of hectorite already swollen beyond the threshold separation as obtained by molecular dynamic simulation (NVT, 300 K). Red bars represent the plane of basal oxygen atoms of the tetrahedral layers. The five blue gaussians are the deconvoluted peaks of the Na^+ locations. Reproduced with permission.^[17] Copyright 2016, American Chemical Society.

This means that all available solvent molecules are incorporated between the nanosheets, giving a maximum separation distance, which indicates a repulsive interaction. If the separation as a function of clay volume fraction holds the h/Φ relationship for a given clay, this is sound experimental evidence for its complete delamination by spontaneous 1D dissolution.

At this point, the nanosheets remain parallel to each other and are not able to rotate because of the much smaller separation between them relative to the diameter of individual nanosheets. This point also reflects the formation of a uniform, nematic liquid crystalline suspension as the single phase. The onset of 1D dissolution at the threshold separation of 2D ionic crystals therefore corresponds to a phase transition from a crystalline swollen phase with discrete d-spacing that corresponds to the molecular dimensions of its interlayer species to a nematic liquid crystal with its separation determined by the volume fraction of dispersed clay in a quasicontinuous manner. The yield of delamination is 100% since it is a thermodynamically driven, spontaneous phase transition. Moreover, delamination does not necessarily produce an isotropic suspension. Only with appreciable nanosheet diameter will anisotropic liquid crystals be observed. Even at low volume fractions (<1 vol%), birefringent nematic suspensions are expected for fully delaminated 2D crystals, as high aspect ratio blocks free rotation of nanosheets.

2.2. How to Trigger Delamination by 1D Dissolution

Most materials require exchange with selected interlayer ions to trigger the phase transition from crystalline swelling to 1D dissolution. Synthetic Na-hectorite clay is exceptional inasmuch as the solvation enthalpy of the interlayer cation is already high enough to take the separation beyond the threshold where repulsive 1D dissolution sets in.^[17] However, it only takes a slight increase of the layer charge from $x = 0.5$ (hectorite) to $x = 0.7$ (vermiculite-type, $[\text{Na}_{0.5}]^{\text{inter}}[\text{Mg}_{2.5}\text{Li}_{0.5}]^{\text{oct}}[\text{Si}_4]^{\text{tet}}\text{O}_{10}\text{F}_2$ and $[\text{Na}_{0.7}]^{\text{inter}}[\text{Mg}_{2.3}\text{Li}_{0.7}]^{\text{oct}}[\text{Si}_4]^{\text{tet}}\text{O}_{10}\text{F}_2$, respectively) and the increased Columbic interactions between charged nanosheets and interlayer ions are too strong to reach the threshold with only the hydration of interlayer cations. In this case, the threshold separation can nevertheless be reached with the help of a steric pressure exerted by bulky interlayer cations.^[18]

1D dissolution is a complex process, where numerous processes occur simultaneously. We adopt a (over-) simplified scheme frequently used to describe dissolution of an ionic crystal by separating the total process into individual steps: We start with unsolvated ionic layered tactoids being dispersed in solvent (Figure 5a). To separate solvent molecules an infinite distance away from charged nanosheets and interlayer ions (Figure 5c), two steps are required both being endergonic. First, the nanosheets and interlayer ions must be separated from each other (cohesion energy) (Figure 5b). Second, intermolecular interactions of solvent molecules must be broken (Figure 5c). These two unfavorable steps are compensated by the solvation energy of both interlayer ions and the basal surfaces of nanosheets. If the solvation energies are larger, the 2D ionic tactoid is spontaneously dissolved in the stacking direction (1D dissolution, Figure 5e). However, if the solvation energies

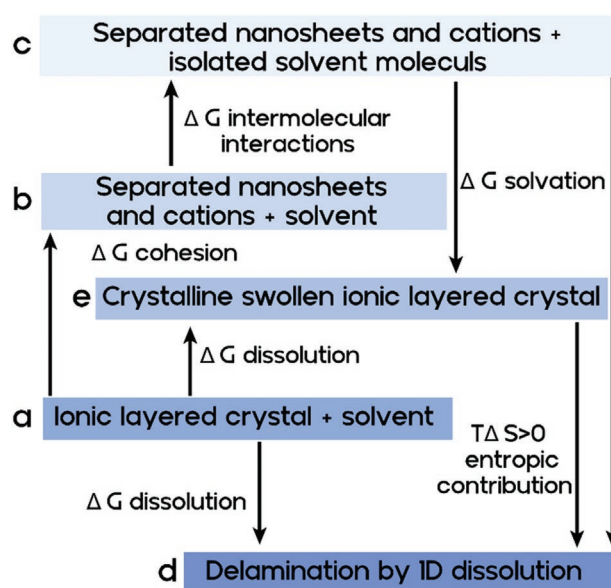


Figure 5. Thermodynamic scheme of 1D dissolution a). Ionic layered tactoid immersed into solvent. b) Increase of free energy upon separation of the nanosheets denoted as energy of cohesion. c) Increase of free energy upon breaking of the interaction between solvent molecules denoted as energy of intermolecular interactions. d) Decrease of free energy upon solvation of ionic layered crystal with solvent molecules, leading to crystalline swollen ionic layered crystal. e) Decrease of free energy upon 1D dissolution.

are smaller we will end up with a crystalline swollen, ionic layered solid tactoid, where its interlayer cations are solvated (Figure 5d). The entropy of the 1D dissolved state is higher than that of the crystalline swollen state dispersed in excess solvent. 1D dissolution can be made favorable by increasing the temperature.^[34] The cohesion energy may be lowered by either reducing the layer charge or by exchange with bulky ions since the leading term of cohesion is Columbic in nature. The layer charge density of nanosheets is therefore one key for 1D dissolution. As a general rule of thumb, the more highly charged the solids are, the more difficult it is to delaminate due to stronger electrostatic attraction. For example, 1D dissolution in water is possible for low-charged 2:1 layered silicates with a charge density of <2.3 charges nm^{-2} and Na^+ as the interlayer cation (e.g., synthetic hectorite^[17] or certain natural, purified montmorillonites^[14a]). Charge densities >2.3 charges nm^{-2} prevent 1D dissolution due to excessive electrostatic attraction.^[18a] In 2:1 layered silicates like hectorite or montmorillonite that carry no acidic groups at the basal surface, the layer charge can be lowered by the so-called Hofmann–Klemen^[35] effect, where small interlayer cations migrate into empty octahedral sites of the 2:1-layer.^[36] In layered crystalline silicic acids and in the zeolites that carry silanol groups at the basal surfaces, the pH of the dispersion modifies the charge density via the degree of protonation of these acidic groups. The same applies to layered metal oxides that carry acidic groups at the basal surface like titanates of lepidocrite type or niobates of layered Ruddlesden–Popper type oxides.^[37]

As previously described, cohesion can be significantly reduced by increasing the d-spacing, particularly through

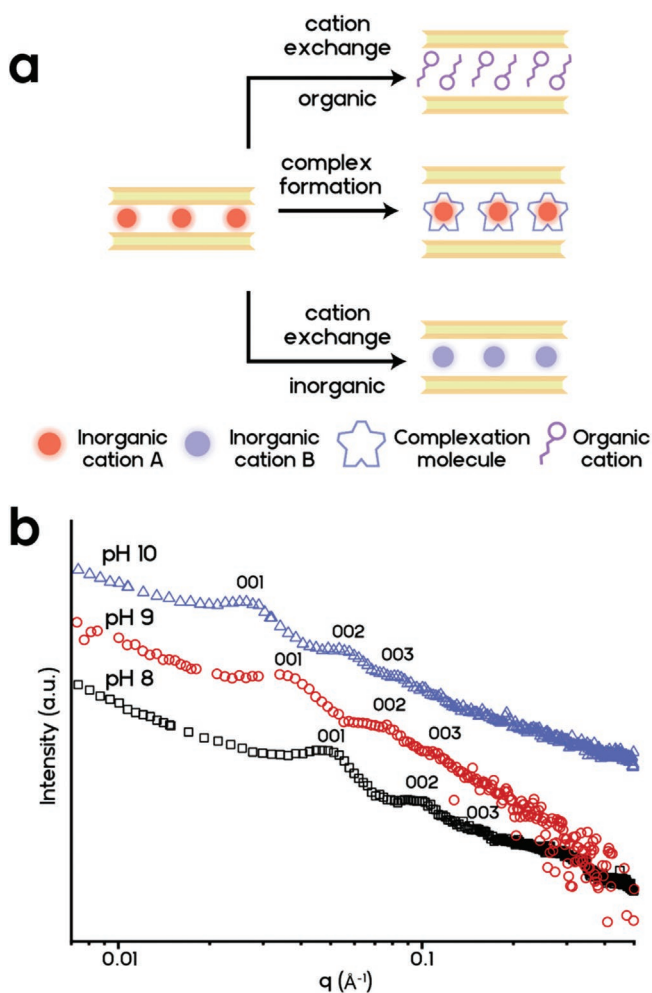


Figure 6. a) Approaches that help to push layered materials above the threshold separation and thus triggering 1D dissolution. b) SAXS curves of Ilerite suspensions recorded at different pH values.

exchange with bulky ions, where bulky means that the charge density of the interlayer ion (equivalent area) is lower than the charge density of the nanosheets.^[38] For such combinations, charge compensation forces the interlayer ions to push the nanosheets further apart increasing the interlayer height and thus weakening cohesion (Figure 6a). A similar expansion of interlayer height may be obtained by complexation of inorganic interlayer cations. Needless to say, ion exchange will also significantly modify the solvation energy. Bulky ions with low solvation energy will not favor 1D dissolution.^[18] Suitable cations offering sufficient bulkiness and high solvation energy that have been successfully applied to delaminate by 1D dissolution are listed in Table 3 together with their charge equivalent areas.

Applying available crystallographic data together with the structural compositions, the charge density of various ionic layered compounds was calculated and also listed in Table 3. Please note that some of the cations listed in Table 3 represent buffer systems.^[39] If these are used in combination with layered compounds that carry acidic groups at the basal surface, the charge density of the layers will be modified according to

the effective pH in the suspension. In Table 3, we assumed a degree of protonation derived from the structural formula as obtained at pH of synthesis. Moreover, the pH for quaternary amines may be altered by additionally adding a base.

The organic base has a decisive impact on the swelling process and can affect the morphology and properties of the final nanosheet suspension. For example, layered titanates intercalated with 2-(dimethylamino)ethanol (DMAE) produced a stable and reversible 100-fold expansion within the interlayer gallery.^[40]

In contrast to the small Li^+ and Na^+ ions, the organic ions mentioned have charge equivalent areas that systematically exceed the charge equivalent areas of the layered compounds. In other words, organic cations capable of triggering 1D dissolution have charge equivalent areas larger than the charge density of the layered compound. For the rather low charged $\text{H}_{0.13}^{\text{inter}} \text{Mn}^{\text{III/IV}} \text{O}_2$ (1.8 charge nm^{-2}), the sterically demanding TBA (1.1 charge nm^{-2}) is needed to trigger 1D dissolution. For more highly charged layer compounds, several significantly smaller organocations are known to trigger 1D dissolution. $\text{H}^{\text{inter}} \text{Ca}_2 \text{Nb}_3 \text{O}_{10}$ (6.7 charge nm^{-2}), for example undergoes 1D dissolution with the much smaller TMA (3.4 charge nm^{-2}) as the interlayer ion (Table 3).

The subtle interplay between effective pH of the suspension, charge density, and steric pressure triggering 1D dissolution can best be illustrated with the recently published example of delamination of Ilerite ($\text{Na}_8[\text{Si}_{32}\text{O}_{64}(\text{OH})_8] \cdot 32 \text{H}_2\text{O}$), also known as NaRUB-18 or octosilicate.^[49] As for 2D zeolites, the 50% deprotonated sodium form, derived from the crystalline silicic acid, contains acidic OH-groups that are exposed at the basal surfaces of the layers giving a layer charge that will consequently alter the pH (Table 3). Thus, ion exchange at a certain pH, where Ilerite is stable, while the amine applied as counter cation is protonated, can be used to examine the influence of the pH on the layer charge and the resulting swelling/dissolution behavior. With decreasing pH, silanol groups become increasingly protonated resulting in a lowering of the layer charge density. For correlating the layer charge density with pH and swelling/dissolution tendency, charge equivalent areas for Ilerite basal surfaces were calculated. The calculated charge equivalent areas at pH 7, 8, 9, and 10 of Ilerite (1.12, 1.37, 1.43, and 1.54 charge nm^{-2} , respectively) decrease by 27%. To trigger delamination by 1D dissolution, the charge equivalent area of the interlayer cation should be larger than that of the layered material. To meet this criterion, a bulky cation is needed that remains protonated at higher pH values. Meglumine (charge equivalent area: 1.30 charge nm^{-2}) was found to be appropriate, particularly as this amino-sugar also offers strong hydrogen bonding to water serving as a swelling agent, which allows for a high solvation energy. For meglumine-ilerite at pH of 7, 8, 9, and 10 the ratio of charge equivalent areas of meglumine to Ilerite is 0.87, 1.06, 1.09, and 1.18, respectively, suggesting that steric pressure will be exerted at a pH above 7. As the solvation energy for this cation is also sufficient, delamination into nanosheets by 1D dissolution could indeed be observed at $\text{pH} > 8$. (reference ilerite paper in press) The onset of the phase transition into the nematic liquid crystalline phase as a function of pH, along with the accompanying delamination and the separation

Table 3. Some 1D dissolved combinations of organo-cations (Cation) and layered compounds: To trigger repulsive osmotic swelling, the cation must be intercalated into the respective layered compound by cation exchange. The cations are TBA, DMAE, C4 (n-butylammonium), C3 (n-propylammonium), and TMA. In the case of hydroxonium-intercalated layer compounds, the cation exchange is carried out by the corresponding tertiary amines as the base, or for quaternary ammonium ions by their hydroxide salts as the base.

	Cation	Name/chemical formula (before cation exchange) ^{a)}	Charge density [charges nm ⁻²]	Charge density of layered compound ^{b)} [charges nm ⁻²]	Ratio ^{c)}
1	TBA	Birnessite ^[41] H _{0.13} ^{inter} MnO ₂	1.1	1.8	1.6
2	TBA	Calciumniobate ^[42] H ^{inter} Ca ₂ Nb ₃ O ₁₀	1.1	6.7	6.0
3	TBA	Lepidocrite type Titanate ^[37b,43] H _{0.8} ^{inter} Ti _{1.2} Fe _{0.8} O ₄	1.1	7.1	6.4
4	TBA	α-Zirconiumphosphate ^[44] Zr(H ^{inter} PO ₄)	1.1	8.3	7.5
5	DMAE	Calciumniobate ^[42] H ^{inter} Ca ₂ Nb ₃ O ₁₀	2.6	6.7	2.5
6	DMAE	Lepidocrite type Titanate ^[37b] H _{0.8} ^{inter} Ti _{1.2} Fe _{0.8} O ₄	2.6	7.1	2.7
7	C4	Vermiculite ^[45] Na, Mg _{x=0.64} ^{inter} [Mg _{2.36} Fe _{0.48} Al _{0.16}] ^{10ct} < Si _{2.72} Al _{1.28} > ^{tetr} O ₁₀ (OH) ₂	2.6	2.6	1.0
8	C3	Caliumhexaniobate ^[46] K ₄ ^{inter} Nb ₆ O ₁₇	3.2	7.1	2.2
9	TMA	Calciumniobate ^[42] H ^{inter} Ca ₂ Nb ₃ O ₁₀	3.4	6.7	1.9
10	TBA	MCM-56 ^[47] 1xSiO ₂ :0.04xAl ₂ O ₃ :0.093xNa ₂ O:0.3xHMI:16 H ₂ O	1.1	1.4	1.3
11	Meglumine	Ilerite Na ₈ [Si ₃₂ O ₆₄ (OH) ₈]:32 H ₂ O (pH 10)	1.5	1.3	1.2

^{a)}The maximum projected area of the cations (calculation: Chemicalize.com^[48]) was taken as the charge equivalent area. The charge equivalent areas for C4 and C3 were taken from literature^[37a]; ^{b)}Calculated for the given compositions and the quoted structural 2D dimensions. For compounds with acidic groups the degree of protonation was assumed as represented by the structural formula obtained at the pH of synthesis. Charge density of vermiculite was calculated by a formula given in literature: 24 Å²/x^[18a]; ^{c)}Ratio of charge density of layered compound and counter cation used for 1D dissolution.

of nanosheets to large distances, can easily be followed by small angle X-ray scattering (SAXS). With meglumine as counter-ion and in the pH range 8–10, spontaneous 1D dissolution results in a nematic phase with separation of adjacent nanosheets >13 nm, while at pH of 7, only a crystalline swollen suspension of ilerite in excess water was obtained. For gels of meglumine-ilerite at pH 8, 9, and 10 with concentrations of 6.3, 7.0, and 2.8 wt%, respectively, a rational 00l series in the SAXS pattern with a periodicity of 12.8, 17.4, and 24.2 nm, respectively, was observed (Figure 6b).

The solvation energy of interlayer ions that is concomitantly modified with steric pressure can best be illustrated by comparing the behavior of Na-hectorite exchanged with different alkali cations ([Alk_{0.5}]^{inter}[Mg_{2.5}Li_{0.5}]^{10ct}[Si₄]^{tet}O₁₀F₂). With Alk⁺ being of high hydration enthalpy, Li⁺ or Na⁺ (519 and 409 kJ mol⁻¹, respectively), 1D dissolution is observed. With Alk⁺ being K⁺, Ru⁺, or Cs⁺ (322 kJ mol⁻¹ and lower),^[50] rather gives crystalline swollen suspensions (Figures 3 and 5e).

The solvation energy can, of course, also be decisively modified by changing the dispersion medium. The most important solvent parameters for triggering 1D dissolution seem to be dielectric constant, dipole moment, and the ability to form hydrogen bonding.^[38,51] Until recently, only water and aqueous solvent mixtures had been established for 1D dissolution. By optimization of the solvent combination, the content of water

could be reduced down to 3 vol%.^[51a] In order to finally realize 1D dissolution in completely water-free media, complexation of interlayer cations proved necessary. Upon complexation of the interlayer cation in synthetic Na-hectorite by crown ethers, which have a high complex building constant with Na⁺, 1D dissolution could successfully be extended for the first time into organic solvents, namely highly polar solvents like propylene carbonate, ethylene carbonate, glycerol carbonate, methyl formamide, methyl acetamide.^[38]

The mastery of spontaneous delamination by 1D dissolution lies in finding the appropriate balance between the charge of the layered material, the properties of the interlayer ion (solvation energy, equivalent area), and the properties of the solvent.

2.3. Assets of Delamination via 1D Dissolution

1D dissolution is restricted to ionic layered solids including ionic transition metal oxides (Ti, Mn, Co, and other),^[37c,52] layered antimony phosphates,^[53] graphene oxide,^[54] layered zeolites,^[55] layered silicates,^[14a,16a–c,23,56] specially treated dichalcogenites,^[57] Ruddlesden–Popper perovskites,^[58] layered-double hydroxides,^[59] and beidellite and nontronites,^[60] but the list steadily increasing (Table 4).

Table 4. Nanosheet characteristics of layered compounds mentioned in the text.

Compound	Group	Basal planes	Porosity of nanosheets	Source of nanosheet charge	Special features
Birnessite $H_{0.13}^{inter} MnO_2$	Hydrous manganese dioxide	Acidic	Impermeable	Deprotonation	Semiconducting, redox active
Calciumniobate ^[39] $H^{inter} Ca_2Nb_3O_{10}$	Ruddlesden–Popper perovskites	Inert	Impermeable	Isomorphous substitution	Semiconducting, photocatalytic, dielectric
Lepidocrite type Titanate $H_{0.8}^{inter} Ti_{1.2}Fe_{0.8}O_4$	Transition metal oxides	Inert	Impermeable	Isomorphous substitution	Semiconducting, photocatalytic, ferromagnetic
α -Zirconiumphosphate $Zr(H^{inter} PO_4)$	Layered acid	Acidic	Impermeable	Deprotonation	Solid-state ion conductive
Na-Hectorite $[Na_{0.5}]^{inter}[Mg_{2.5}Li_{0.5}]^{oct}[Si_4]^{tet}O_{10}F_2$	2:1 clay	Inert	Impermeable	Isomorphous substitution in octahedral or tetrahedral layer	Insulating, high aspect ratio
Illerite $Na_8[Si_{32}O_{64}(OH)_8] \cdot 32 H_2O$	Na-silicate	Acidic	Microporous	Deprotonation	Insulating, well-defined nanoporosity
Vermiculite $Na, Mg_{x=0.64}^{inter}[Mg_{2.36}Fe_{0.48}Al_{0.16}]^{oct} <Si_{2.72}Al_{1.28}>^{tet}O_{10}(OH)_2$	2:1 clay	Inert	Impermeable	Isomorphous substitution in octahedral layer	Insulating, high temperature resistant, Fenton's reagent
Caliumhexaniobate $K_4^{inter} Nb_6O_{17}$	Ruddlesden–Popper perovskites	Inert	Impermeable	Isomorphous substitution	Dielectric, photocatalitic
layered antimony phosphates $H_3^{inter} Sb_3P_2O_{14}$	layered acid	Acidic	Impermeable	Deprotonation	Insulating, ion-conductive
MCM-56, $1xSiO_2 \cdot 0.04xAl_2O_3 \cdot 0.093xNa_2O \cdot 0.3xHMI : 16 H_2O$	layered zeolites	Acidic	Microporous	Isomorphous substitution in tetrahedral layer	Insulating, well-defined nanoporosity
Graphene oxide $C_xH_yO_z$	Carbon based	Acidic	Microporous	Deprotonation	Insulating, high degree of functionality
Beidellite $(Na, Ca_{0.5})_{0.3}Al_2(Si, Al)_4O_{10}(OH)_2 \cdot 4H_2O$	2:1 clay	Inert	Impermeable	Isomorphous substitution in octahedral or tetrahedral layer	Insulating, high temperature resistant
Nontronite $(CaO_{0.5}, Na)_{0.3}Fe^{3+}_2(Si, Al)_4O_{10}(OH)_2 \cdot nH_2O$	2:1 clay	Inert	Impermeable	Isomorphous substitution in octahedral or tetrahedral layer	Insulating, high temperature resistant, fenton's reagent

The biggest assets of 1D dissolution is derived from the thermodynamically allowed, exergonic nature of the spontaneous, repulsive process (Figure 7). As a consequence,

1. The material (ideally) is delaminated completely into individual, single-layer nanosheets, thus providing the necessary atomic efficiency for a sustainable application of 2D materials.
2. Being repulsive in nature, 1D dissolution is the softest delamination method, allowing for preservation of the aspect ratio of the pristine material and enhanced anisotropy, which is one of the key qualities of interest for 2D materials. For instance, the titanate nanosheets delaminated by 1D dissolution showed a lateral size of 5 μm and monolayer thickness,^[37a] while the same material exfoliated via liquid phase exfoliation following ion exchange to increase shear lability resulted in substantial smaller lateral dimensions of roughly 1 μm and a mean thickness of 75 nm.^[61] As only mild conditions are required, the process is energy efficient and does not introduce additional defects to the structure of nanosheets. This renders them most appropriate for advanced applications that require high purity and defect-free structures.
3. The repulsive nature automatically leads to an electrostatically stabilized suspension. With appreciable diameters of

>100 nm, even dilute suspensions of >1 vol% yield liquid crystalline phases. Nematic liquid crystals offer an enormous opportunity to manipulate the orientation and morphology of the material with various external fields to hold the nanosheets coplanar within domains. The statistically oriented individual domains can easily be oriented into monodomains by electrostatic,^[62] magnetic,^[63] or simple shear forces.^[64]

3. Application

3.1. Barrier Coatings

Various products ranging from food to pharmaceutical to (opto-) electronic devices require protection from various gases.^[65] For instance, reactions with oxygen spoil food products and promote corrosion in metals, while water vapour reacts with the components of electronic devices. To mitigate the effect of gas molecules, various protective coatings have been applied.^[66] One of the most efficient barrier coatings are nanocomposites based on impermeable, 2D nanosheets.^[67]

To establish a severe tortuous path that retards permeation, which is the mechanism responsible for the outstanding

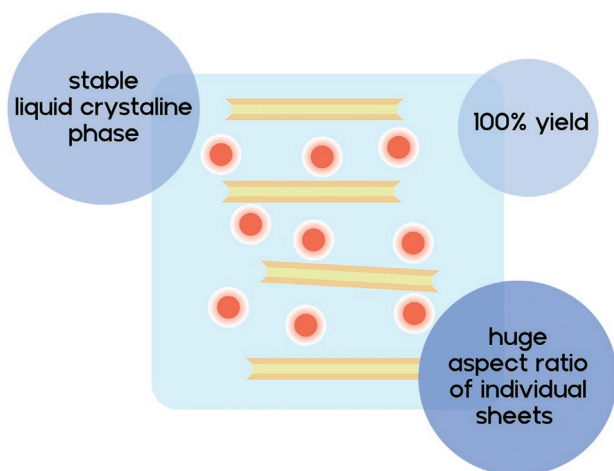


Figure 7. Key features of 1D dissolution. A nematic liquid crystalline phase is obtained with uniform separation of coplanar nanosheets, complete delamination with 100% yield of single nanosheets in a soft dissolution, allowing to preserve the aspect ratio inherent to the diameter of the pristine layered crystal.

performance of nanocomposite barriers, three main parameters are important: orientation of the filler within a polymer matrix, the volume fraction of impermeable filler, and most importantly, the filler aspect ratio.^[67a] 1D dissolution maximizes the values for all three of these parameters. Aspect ratio is maximized due to soft delamination, allowing for the creation of nanosheets with an aspect ratio up to 20 000.^[23] High aspect ratio also fosters orientation of the nanosheets parallel to a planar substrate by anchoring the nanosheets to the surface.^[68] The liquid crystalline nature allows processing the nanocomposite from the liquid suspension phase via common industrial methods including spray coating, doctor blading, roll-to-roll or slot die coating.^[69] The mild shear forces exerted in these processes are fully sufficient for orienting the nanosheets parallel to the substrate and achieving the perfect orientation (texture) parallel to the substrate.^[64] The solution processability allows for nanocomposites with very high volume fractions of filler simply by varying the ratio between polymer and filler in the suspension. Nanocomposites with record filler contents of 91 wt%^[6a] can be routinely prepared with this approach. For selected polymer matrices like polyethyleneglycol, polyvinylalcohol, and polyvinylpyrrolidone,^[6,69a,70] even monodomain coatings (Bragg stacks) with periodic arrangement of filler and polymer chains are obtained. These Bragg stacks are transparent and allow for characterisation by Brillouin light scattering and thermal conductivity.^[6]

Other more commonly applied nanosheets for composites like laponite or montmorillonite have insufficient diameters to meet high barrier demands in applications like optoelectronics or sensitive food due to their low intrinsic aspect ratio. Higher aspect ratio synthetic^[50] or natural clays (reference vermiculite paper submitted) can be accessed by 1D dissolution to produce suitable coatings with much higher barrier compared to composites of common nanosheets. For example, synthetic hectorite composite coatings outperform montmorillonite by almost 20 times.^[22a,71]

High barrier composite coatings of synthetic hectorite delaminated by 1D dissolution can be prepared with various

commercial polymers to achieve transparent and flexible coatings with oxygen transmission rate (OTR) and water vapor transmission rate (WVTR) values as high as $10^{-2} \text{ cm}^3 \text{ m}^{-2} \text{ day}^{-1} \text{ bar}^{-1}$ and $<0.05 \text{ g m}^{-2} \text{ day}^{-1}$ at 50% relative humidity (RH), respectively,^[69b] making them suitable for optoelectronic applications. Biodegradable barrier coatings represent a great challenge as many biodegradable polymers inherently have very high permeability, particularly at elevated RH. In this context, thin hectorite-chitosan coatings are capable of reducing the OTR of a poly(lactic acid) (PLA) substrate from $874.2 \text{ cm}^3 \text{ m}^{-2} \text{ day}^{-1} \text{ bar}^{-1}$ to $0.08 \text{ cm}^3 \text{ m}^{-2} \text{ day}^{-1} \text{ bar}^{-1}$.^[72] Although these barrier coatings are water-born, surprisingly low OTR and WVTR at 90% RH for a coating of $0.42 \mu\text{m}$ was achieved ($0.11 \text{ cm}^3 \text{ m}^{-2} \text{ day}^{-1} \text{ bar}^{-1}$ and $0.18 \text{ g m}^{-2} \text{ day}^{-1}$, respectively).^[69a,73] In particular, delaminated natural vermiculite clays as obtained by 1D dissolution offer great potential for improving the barrier properties of bio-sourced, sustainable, and biodegradable foils to the level required for ambitious food packaging applications. Nanocomposite coatings of degradable polyesters on water-soluble cellulose substrates exhibited OTR and WVTR of $1.42 \text{ cm}^3 \text{ m}^{-2} \text{ day}^{-1} \text{ atm}^{-1}$ and $1.17 \text{ g m}^{-2} \text{ day}^{-1} \text{ atm}^{-1}$, respectively, which outperforms high-end, nondegradable poly(vinylidene dichloride) foils. Vermiculite could potentially be the key to simultaneously mitigating the two major drawbacks associated with biodegradable plastics, i.e., price and poor properties, fostering their wider implementation and thus contributing to addressing the ubiquitous microplastic challenge (reference vermiculite paper submitted).

Moreover, the tortuous path approach slows down diffusion of even the most mobile gases, i.e., helium and hydrogen, which is highly relevant for containers needed in the hydrogen economy.^[74] Corrosion resistance is also improved by the 2D nanosheets created through 1D dissolution using the transition metal oxides^[75] or natural vermiculites.^[76]

3.2. Hydrogels

Hydrogels are vital materials for soft robotics and biomedical research. They consist of a cross-linked polymer network that swells in water while maintaining a defined morphology. Similar to tissues in the human body, hydrogels consist mostly of water.^[77] The mechanical properties of hydrogels are close to that of real human tissues, promoting their compatibility.^[78] Different tissues have different mechanical properties, which means there exists no single universal gel that is suitable for every application. One of the effective ways to increase the mechanical properties of hydrogels is reinforcement with fillers, i.e., nanocomposite hydrogels.^[79] In this context, nanosheets obtained by 1D dissolution have great potential.

Electrostatic repulsion between nanosheets in the nematic liquid crystalline phase increases the homogeneity of polymer network, which may boost the mechanical performance of the nanocomposite hydrogel, in addition to the direct reinforcement provided by the mechanically strong filler.^[79a]

Anisotropic soft materials are ubiquitous in nature but it is challenging to fabricate them.^[80] The anisotropic properties

of nematic suspensions of nanosheets can easily be translated into anisotropic nanocomposite hydrogels through macroscopic alignment of nanosheets via external fields. The first hydrogel of this type was prepared from a 2D nanosheet suspension produced from 1D dissolution of a layered titanate.^[81] Similar to articular cartilage, negatively charged nanosheets induce an unusual mechanical behaviour of the material. While it is easily deformed under shearing, it resists compression. Anisotropic properties could be enhanced even further by decreasing the number of ionic contaminants and choosing an appropriate polymer matrix with interior permittivity to boost the anisotropic ratio up to 85.^[82] The addition of gold nanoparticles to this nanosheet hydrogel allows for local heating, which in turn can trigger controlled locomotion, mimicking the peristaltic movement of worms.^[83] A combination of this nanosheet suspension with polymer matrices with a lower critical solution temperature like poly(N-isopropylacrylamide), allows for fabrication of nanocomposite hydrogel actuators. These hydrogels showed the largest and fastest deformation known without substantial water uptake and release, and can be programmed to proceed unidirectionally through internal conversion of isotropic energy into a directional mechanical motion.^[84]

The polycrystalline domains of nematic phase of Na-hectorite can easily be oriented, even into complex patterns, by applying electric field patterns created by distributed electrodes (Figure 8a). This property allows for mimicking the anisotropic properties of muscles. To achieve oriented nanocomposite structures, nematic suspensions were mixed with N-isopropylacrylamide monomers and the domains were oriented by patterned electric fields during polymerization.^[62a] This way, a nanocomposite hydrogel is obtained that exhibits muscle-like behavior with programmable deformations. The electric field patterns may be realized by either multiple point electrodes^[62c] (Figure 8b) or by multistep electrode^[62b] assisted orientation of the nanosheets (Figure 8c).

3.3. Materials for Optics and Electronics

2D materials have unique electronic and optical properties owing to the 2D confinement of electrons in the nanosheet lattice. The full range of electronic structure types are available with materials ranging from semimetals^[85] to semiconductors^[37c] to insulators^[23] with large bandgap, enabling a wide selection of potential novel applications. 1D dissolution additionally offers the solution-based processability facilitating easy production of printable electronics, while the metal–oxide–semiconductor interfaces may resemble structures similar to what is required of conventional integrated circuits. These features, in principle, allows unlimited possibilities to apply toward an improved performance of optoelectronic devices.

Compared to conventional van der Waals crystals, nanosheets obtained by 1D dissolution may furthermore be combined with charged molecules like cationic dyes or nanoparticles to add additional functionality while preserving the liquid crystalline phase and thus, processibility. As hydrophobic cationic dyes strongly adsorb to the nanosheet surface, ion exchange is limited to a few percent of the exchange capacity to avoid flocculation of the electrostatically stabilized nematic phase.^[86] Alternatively, such dyes may be sandwiched between two nanosheets, while these double stacks undergo 1D dissolution into a nematic phase (Figure 9). Confining the dye molecules between two nanosheets forces the molecules into a preferred orientation, which leads to directional emission properties when cast into films.^[87] Moreover, the sandwich shows increased thermal stability and increased emission lifetime.^[88]

As with dyes, colloidal objects could also be sandwiched between two nanosheets in a double stack. With magnetic nanoparticles, ferronematic liquid crystalline phases are obtained that may be oriented even by very weak magnetic fields of 5 mT. Moreover, the magnetic properties can be tuned independently of the material chemistry simply by varying the ratio between nanoparticles and nanosheets.^[63a]

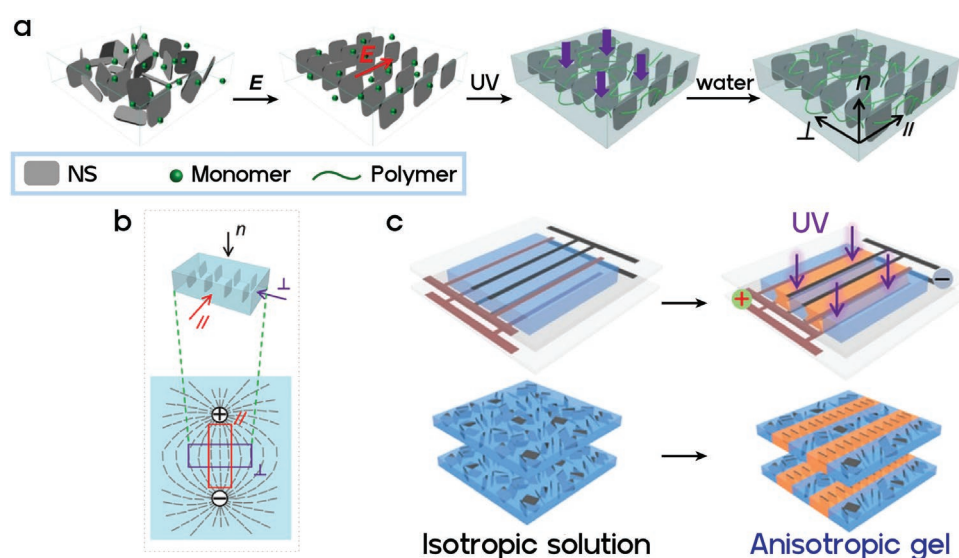


Figure 8. Methods for preparation of anisotropic gels using nanosheets obtained from 1D dissolution. a) Electrode assisted fabrication. Reproduced with permission.^[62c] Copyright 2020, Springer Nature. b) Multiple point electrodes. Reproduced with permission.^[62c] Copyright 2020, Wiley-VCH GmbH. c) Multistep electrode assisted fabrication. Reproduced with permission.^[62a] Copyright 2021, Wiley-VCH GmbH.

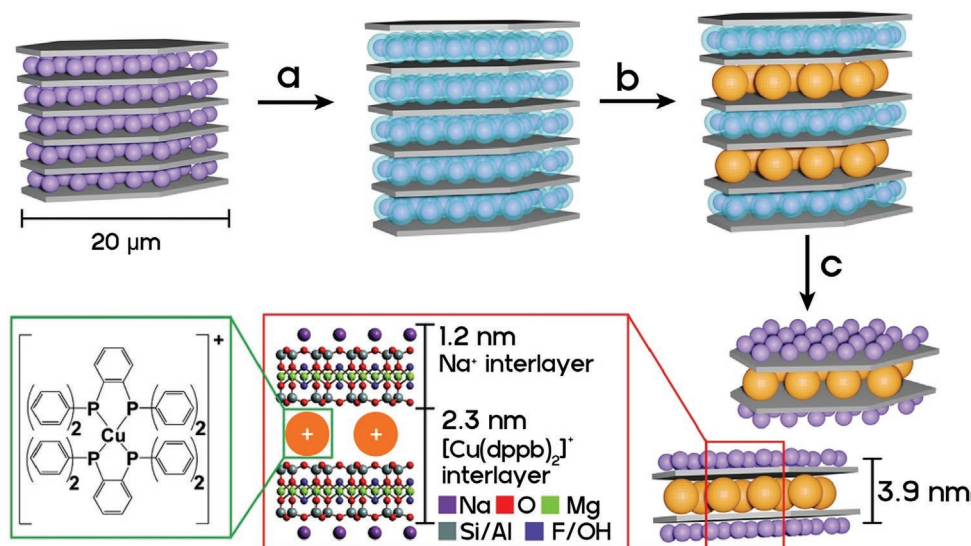


Figure 9. Synthetic procedure for the encapsulation of $[\text{Cu}(\text{dbbp})_2]^+$ into Na^+ -hectorite. a) Crystalline swelling in 75 vol% acetonitrile. b) Partial exchange of Na^+ layers by $[\text{Cu}(\text{dbbp})_2]^+$ layers with the formation of ordered heterostructures (at a cationic exchange ratio of 22% CEC), and c) complete delamination of double-stacks encapsulating the hydrophobic $[\text{Cu}(\text{dbbp})_2]^+$ ions between two silicate layers. Reproduced with permission.^[88] Copyright 2021, Wiley-VCH GmbH.

3.4. Photonic Crystals for Structural Coloration

As the interaction of nanosheets in the nematic phase is of repulsive Coulomb type, the separation can be readily increased into the range of visible light wavelengths by adding appropriate amounts of dispersion medium forming a photonic crystal. A photonic crystal is an optical nanostructure in which the refractive index changes periodically resulting in a photonic bandgap according to the Bragg–Snell law.^[89] Periodicity can reach the micrometer scale without losing the coplanar arrangement of nanosheets in domains. Moreover, monodomain suspensions may be obtained by orientation of the nanosheets in electromagnetic fields. Structural coloration was already demonstrated for niobates,^[90] titanates^[63b] (Figure 10a), and clays^[91] (Figure 10b). Unlike traditional structural colors, this mesophase is dynamic and can be tuned by numerous stimuli like pH,^[63b] temperature,^[63b] ionic strength of solution,^[91a] or adsorption of a polymer.^[92] This unique liquid mesophase can be solidified by applying a hydrogel matrix and the resulting nanocomposites are capable of a chromomechanical response.^[93]

When this unique mesophase is structured into a single domain Bragg stack, the separation between nanosheets is governed by the balance between electrostatic repulsion and van der Waals interactions. Upon changing this balance by injecting a NaCl-solution or gaseous CO_2 , the electrostatic repulsion could be modulated enabling the photonic phase to undergo a coherent motion that can be used for long-range directional transport of microparticles.^[94]

3.5. Superion Conducting Channels

At a high concentration of nematic phases, the slits between the adjacent nanosheets impose a severe confinement onto solvated counter ions. This confinement, in conjunction with the

reduced dimensionality, may trigger unexpected properties.^[7e,95] By spray coating onto a substrate, self-standing nanosheet films may be prepared and by controlling the content of dispersion medium, films with defined 1D periodicity are obtained. The solvent filled slits between nanosheets represent nanochannels for the counter ions.^[96] The nanofluidic transport of ions confined in such nanoscale channels having a separation range of 1–100 nm causes significant differences in the ion conductivity compared to bulk solutions (Figure 11).^[97] If the dimensions of the channel approach the Debye length, 2D superionic transport enables ionic conductivities to increase by several orders of magnitude compared to the bulk.^[96,97b,98] Not surprisingly given the anisotropy of these films, the conductivities are multiple orders of magnitude higher in-plane compared to cross-plane.^[95a] A variety of ions can be effectively channelled (e.g., H^+ , Li^+ , Na^+ , K^+ , Ca^{2+} , Al^{3+} , OH^-).^[95a,97b,99] At the same time, the individual transport properties can be tailored by choice of the respective 2D material constituting the channels. The surface characteristics of the channel mainly govern the transport properties.^[100] Properties like charge, charge density, channel size, and individual interactions between the nanosheets and the transported ions come into play. The surface charge of the channels will effectively repel the co-ions, while allowing only the counter ions to move through the slits.^[101] While conventional methods employing lithography or sacrificial agents are time-consuming and offer limited possibilities to tailor the nature of the channels, the wide variety of 2D materials and versatility of the 1D dissolution approach enables tailoring of each of these properties individually. Superionic transport in reconstructed channels has been demonstrated for a variety of 2D materials, including GO ^[97b] (H^+ , K^+ , Ca^{2+}), vermiculite^[96] (H^+), LDHs^[95a] (OH^-), boron nitride^[101a] (H^+ , K^+ , Na^+), and MXenes^[99c] (H^+ , Na^+ , K^+ , Al^{3+}).

The possibility of manufacturing high-performance ion conductors/electrolytes from 2D building blocks enables a myriad of applications in sensing, gas separation, fuel cells,

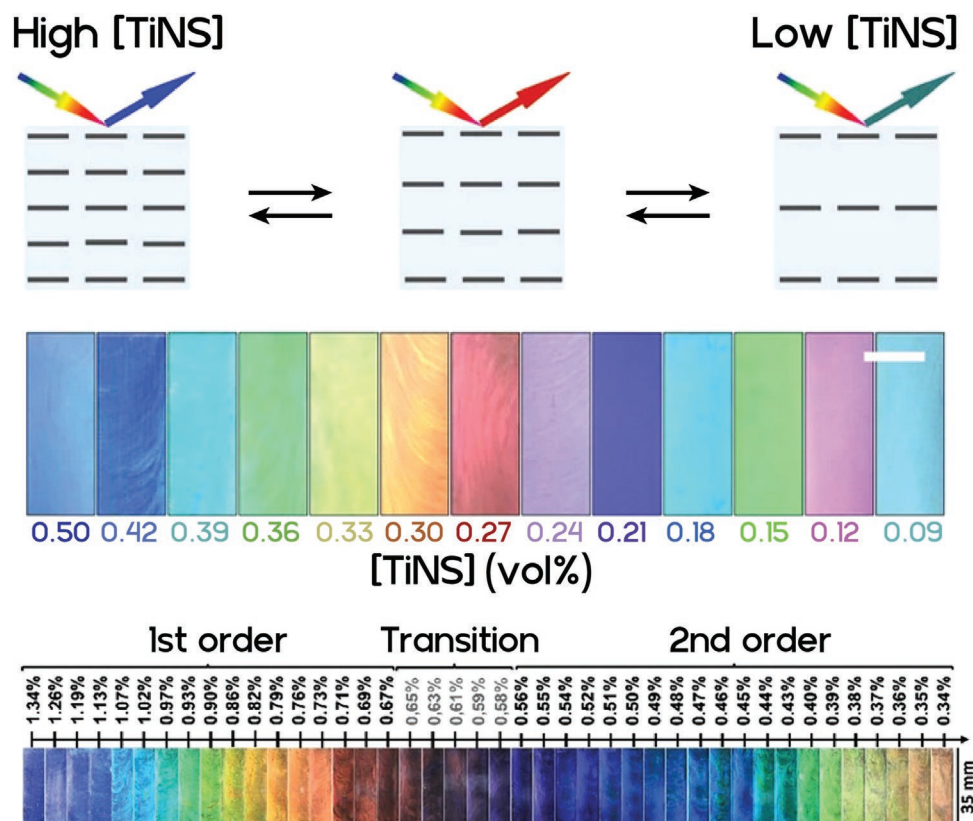


Figure 10. Structural coloration by a nanosheet nematic phase. a) Structural coloration from titanate nanosheets and general principle of color formation. Scale bar 5 mm. Reproduced with permission.^[63b] Copyright 2016, Springer Nature. b) Structural coloration from clay nanosheets.

water electrolysis, and battery materials. For instance, films of 2D materials can act as H^+/OH^- conductors in the case of fuel cells,^[95a,98] or aid the ionic filtration^[100] and recovery of valuable ions.

4. Summary and Outlook

What has historically been named osmotic swelling early as 1930 from work with graphite oxide presents a highly attractive approach for the delamination of layered materials. As we

illustrate in this review, the process actually resembles the dissolution of ionic crystals that is, by the 2D nature of the pristine layered material, restricted to the stacking direction of the nanosheets in the tactoid. Therefore, we suggest to rename it to 1D dissolution instead of osmotic swelling. As 1D dissolution is a thermodynamically driven, spontaneous process, it affords some advantages over the more common liquid phase exfoliation that rely on brute force shearing. 1D dissolution offers an attractive method for the delamination of layered compounds as it maximizes aspect ratio of nanosheets, does not introduce defects during delamination, is atom and energy efficient, and

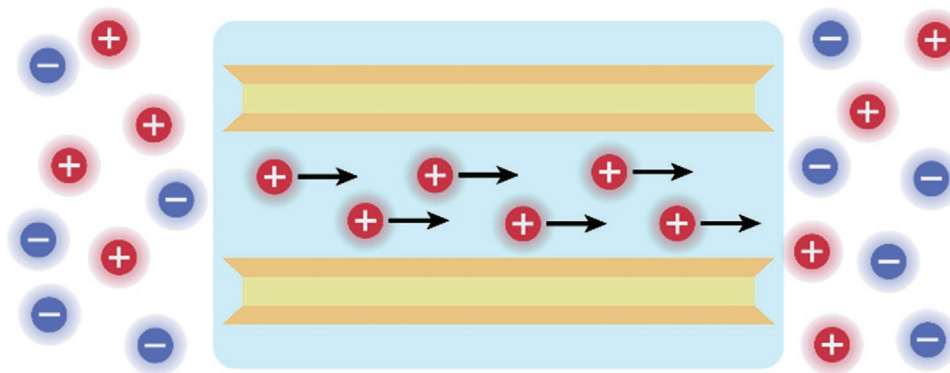


Figure 11. Schematic illustration of superionic conduction in the slit confinement of nematic liquid crystals.

promotes self-assembly as it tends to produce nematic liquid crystalline phases. A fundamental understanding of the underlying processes involved in 1D dissolution will eventually render it generally applicable for different material types and thus offers great potential for new applications.

Unfortunately, 1D dissolution is limited to ionic-layered solids. As many van der Waals crystals like graphite or dichalcogenides can easily be charged by their redox-activity, they might nevertheless be accessible to 1D dissolution in this stage. The dispersion medium must, of course, be stable at the redox potential of the oxidized or reduced layered compound, which might pose a severe restriction.

Acknowledgements

V.D. and O.K. contributed equally to this work. The authors acknowledge support by the Deutsche Forschungsgemeinschaft (DFG, German Research Foundation) – Project No. 391977956 –SFB1357/C02. V.D. thanks the Elite Network of Bavaria for support. They also acknowledge R. Timmins for the English proofreading.

Open access funding enabled and organized by Projekt DEAL.

Conflict of Interest

The authors declare no conflict of interest.

Keywords

1D dissolution, 2D materials, delamination, exfoliation, nanosheets, osmotic swelling

Received: April 5, 2022

Revised: August 11, 2022

Published online: November 6, 2022

- [1] X. Huang, M. A. El-Sayed, *J. Adv. Res.* **2010**, *1*, 13.
 [2] M. Haruta, *Chem. Rec.* **2003**, *3*, 75.
 [3] N. Baig, I. Kammakam, W. Falath, *Mater. Adv.* **2021**, *2*, 1821.
 [4] S. Guo, S. Dong, *Chem. Soc. Rev.* **2011**, *40*, 2644.
 [5] M. Zhao, Y. Huang, Y. Peng, Z. Huang, Q. Ma, H. Zhang, *Chem. Soc. Rev.* **2018**, *47*, 6267.
 [6] a) T. Dörres, M. Bartkiewicz, K. Herrmann, M. Schöttle, D. Wagner, Z. Wang, O. Ikkala, M. Retsch, G. Fytas, J. Breu, *ACS Appl. Nano Mater.* **2022**, *5*, 4119; b) Z. Wang, K. Rolle, T. Schilling, P. Hummel, A. Philipp, B. A. F. Kopera, A. M. Lechner, M. Retsch, J. Breu, G. Fytas, *Angew. Chem., Int. Ed.* **2020**, *59*, 1286.
 [7] a) A. K. Geim, *Angew. Chem., Int. Ed.* **2011**, *50*, 6966; b) K. S. Novoselov, *Angew. Chem., Int. Ed.* **2011**, *50*, 6986; c) A. K. Geim, *Science* **2009**, *324*, 1530; d) A. K. Geim, K. S. Novoselov, *Nat. Mater.* **2007**, *6*, 183; e) K. S. Novoselov, A. K. Geim, S. V. Morozov, D. Jiang, Y. Zhang, S. V. Dubonos, I. V. Grigorieva, A. A. Firsov, *Science* **2004**, *306*, 666.
 [8] a) J. W. Colson, W. R. Dichtel, *Nat. Chem.* **2013**, *5*, 453; b) J. N. Coleman, M. Lotya, A. O'Neill, S. D. Bergin, P. J. King, U. Khan, K. Young, A. Gaucher, S. De, R. J. Smith, I. V. Shvets, S. K. Arora, G. Stanton, H.-Y. Kim, K. Lee, G. T. Kim, G. S. Duesberg, T. Hallam, J. J. Boland, J. J. Wang, J. F. Donegan, J. C. Grunlan, G. Moriarty, A. Shmeliov, R. J. Nicholls, J. M. Perkins, E. M. Grieveson, K. Theuvsissen, D. W. McComb, P. D. Nellist, et al., *Science* **2011**, *331*, 568; c) C. N. R. Rao, H. S. S. R. Matte, U. Maitra, *Angew. Chem., Int. Ed.* **2013**, *52*, 13162; d) H.-P. Cong, J.-F. Chen, S.-H. Yu, *Chem. Soc. Rev.* **2014**, *43*, 7295; e) A. A. Tedstone, D. J. Lewis, P. O'Brien, *Chem. Mater.* **2016**, *28*, 1965; f) C. Tan, X. Cao, X.-J. Wu, Q. He, J. Yang, X. Zhang, J. Chen, W. Zhao, S. Han, G.-H. Nam, M. Sindoro, H. Zhang, *Chem. Rev.* **2017**, *117*, 6225; g) Q. Wang, D. O'Hare, *Chem. Rev.* **2012**, *112*, 4124; h) H. Zhang, *ACS Nano* **2015**, *9*, 9451.
 [9] D. Deng, K. S. Novoselov, Q. Fu, N. Zheng, Z. Tian, X. Bao, *Nat. Nanotechnol.* **2016**, *11*, 218.
 [10] Q. H. Wang, K. Kalantar-Zadeh, A. Kis, J. N. Coleman, M. S. Strano, *Nat. Nanotechnol.* **2012**, *7*, 699.
 [11] D. Tyagi, H. Wang, W. Huang, L. Hu, Y. Tang, Z. Guo, Z. Ouyang, H. Zhang, *Nanoscale* **2020**, *12*, 3535.
 [12] N. Rohaizad, C. C. Mayorga-Martinez, M. Fojtů, N. M. Latiff, M. Pumera, *Chem. Soc. Rev.* **2021**, *50*, 619.
 [13] a) R. Rojaee, R. Shahbazian-Yassar, *ACS Nano* **2020**, *14*, 2628; b) M. Osada, T. Sasaki, *Adv. Mater.* **2012**, *24*, 210; c) J. E. t. Elshof, H. Yuan, P. G. Rodriguez, *Adv. Energy Mater.* **2016**, *6*, 1600355; d) B. Mendoza-Sánchez, Y. Gogotsi, *Adv. Mater.* **2016**, *28*, 6104; e) Q. Zhang, J. Zhang, S. Wan, W. Wang, L. Fu, *Adv. Funct. Mater.* **2018**, *28*, 1802500.
 [14] a) K. Norrish, *Discuss. Faraday Soc.* **1954**, *18*, 120; b) M. Faustini, L. Nicole, E. Ruiz-Hitzky, C. Sanchez, *Adv. Funct. Mater.* **2018**, *28*, 1704158; c) U. Hofmann, A. Frenzel, *Ber. dtsh. Chem. Ges. A/B* **1930**, *63*, 1248.
 [15] W. J. West, *J. Colloid Sci.* **1952**, *7*, 295.
 [16] a) G. F. Walker, W. G. Garrett, *Science* **1967**, *156*, 385; b) W. G. Garrett, G. F. Walker, *Clays Clay Miner.* **1960**, *9*, 557; c) G. F. Walker, *Nature* **1960**, *187*, 312; d) G. F. Walker, *Nature* **1949**, *163*, 726; e) K. Norrish, *Nature* **1954**, *173*, 256.
 [17] S. Rosenfeldt, M. Stöter, M. Schlenk, T. Martin, R. Q. Albuquerque, S. Förster, J. Breu, *Langmuir* **2016**, *32*, 10582.
 [18] a) M. Daab, N. J. Eichstaedt, C. Habel, S. Rosenfeldt, H. Kalo, H. Schießling, S. Förster, J. Breu, *Langmuir* **2018**, *34*, 8215; b) M. Daab, N. J. Eichstaedt, A. Edenharter, S. Rosenfeldt, J. Breu, *RSC Adv.* **2018**, *8*, 28797; c) M. Daab, S. Rosenfeldt, H. Kalo, M. Stöter, B. Bojer, R. Siegel, S. Förster, J. Senker, J. Breu, *Langmuir* **2017**, *33*, 4816.
 [19] a) N. Miyamoto, T. Nakato, *Isr. J. Chem.* **2012**, *52*, 881; b) R. Ma, T. Sasaki, *Adv. Mater.* **2010**, *22*, 5082; c) M. A. Bizeto, A. L. Shiguihara, V. R. L. Constantino, *J. Mater. Chem.* **2009**, *19*, 2512; d) R. Ma, T. Sasaki, *Acc. Chem. Res.* **2015**, *48*, 136.
 [20] A. K. Geim, I. V. Grigorieva, *Nature* **2013**, *499*, 419.
 [21] V. Nicolosi, M. Chhowalla, M. G. Kanatzidis, M. S. Strano, J. N. Coleman, *Science* **2013**, *340*, 1226419.
 [22] a) M. W. Möller, T. Lunkenbein, H. Kalo, M. Schieder, D. A. Kunz, J. Breu, *Adv. Mater.* **2010**, *22*, 5245; b) M. W. Möller, U. A. Handge, D. A. Kunz, T. Lunkenbein, V. Altstädt, J. Breu, *ACS Nano* **2010**, *4*, 717.
 [23] M. Stöter, D. A. Kunz, M. Schmidt, D. Hirsemann, H. Kalo, B. Putz, J. Senker, J. Breu, *Langmuir* **2013**, *29*, 1280.
 [24] C. Backes, *Nature* **2022**, *602*, 582.
 [25] J. E. F. C. Gardolinski, G. Lagaly, *Clay Miner.* **2005**, *40*, 547.
 [26] a) A. Ciesielski, P. Samori, *Chem. Soc. Rev.* **2013**, *43*, 381; b) C. Backes, T. M. Higgins, A. Kelly, C. Boland, A. Harvey, D. Hanlon, J. N. Coleman, *Chem. Mater.* **2017**, *29*, 243.
 [27] L. Niu, J. N. Coleman, H. Zhang, H. Shin, M. Chhowalla, Z. Zheng, *Small* **2016**, *12*, 272.
 [28] A. Wiewióra, J. L. Pérez-Rodríguez, L. A. Perez-Maqueda, J. Drapáta, *Appl. Clay Sci.* **2003**, *24*, 51.
 [29] M. V. Bracamonte, G. I. Laccioni, S. E. Urreta, L. E. F. Foa Torres, *J. Phys. Chem. C* **2014**, *118*, 15455.
 [30] a) Z. Li, R. J. Young, C. Backes, W. Zhao, X. Zhang, A. A. Zhukov, E. Tillotson, A. P. Conlan, F. Ding, S. J. Haigh, K. S. Novoselov,

- J. N. Coleman, *ACS Nano* **2020**, *14*, 10976; b) J. N. Coleman, M. Lotya, A. O'Neill, S. D. Bergin, P. J. King, U. Khan, K. Young, A. Gaucher, S. De, R. J. Smith, I. V. Shvets, S. K. Arora, G. Stanton, H.-Y. Kim, K. Lee, G. T. Kim, G. S. Duesberg, T. Hallam, J. J. Boland, J. J. Wang, J. F. Donegan, J. C. Grunlan, G. Moriarty, A. Shmeliov, R. J. Nicholls, J. M. Perkins, E. M. Grieveson, K. Theuvsen, D. W. McComb, P. D. Nellist, et al., *Science* **2011**, *331*, 568.
- [31] W. Zheng, L. Y. S. Lee, *Matter* **2022**, *5*, 515.
- [32] P. Yu, S. E. Lowe, G. P. Simon, Y. L. Zhong, *Curr. Opin. Colloid Interface Sci.* **2015**, *20*, 329.
- [33] A. Lurf, *Dalton Trans.* **2014**, *43*, 10276.
- [34] E. L. Hansen, H. Hemmen, D. M. Fonseca, C. Coutant, K. D. Knudsen, T. S. Plivelic, D. Bonn, J. O. Fossum, *Sci. Rep.* **2012**, *2*, 618.
- [35] U. Hofmann, R. Klemen, *Z. Anorg. Chem.* **1950**, *262*, 95.
- [36] M. M. Herling, H. Kalo, S. Seibt, R. Schobert, J. Breu, *Langmuir* **2012**, *28*, 14713.
- [37] a) T. Maluangnont, K. Matsuba, F. Geng, R. Ma, Y. Yamauchi, T. Sasaki, *Chem. Mater.* **2013**, *25*, 3137; b) F. Geng, R. Ma, A. Nakamura, K. Akatsuka, Y. Ebina, Y. Yamauchi, N. Miyamoto, Y. Tateyama, T. Sasaki, *Nat. Commun.* **2013**, *4*, 1632; c) T. Sasaki, M. Watanabe, *J. Am. Chem. Soc.* **1998**, *120*, 4682.
- [38] V. Dudko, K. Ottermann, S. Rosenfeldt, G. Papastavrou, J. Breu, *Langmuir* **2021**, *37*, 461.
- [39] T. Sasaki, M. Watanabe, H. Hashizume, H. Yamada, H. Nakazawa, *J. Am. Chem. Soc.* **1996**, *118*, 8329.
- [40] F. Geng, R. Ma, A. Nakamura, K. Akatsuka, Y. Ebina, Y. Yamauchi, N. Miyamoto, Y. Tateyama, T. Sasaki, *Nat. Commun.* **2013**, *4*, 1632.
- [41] a) Y. Omomo, T. Sasaki, Wang, M. Watanabe, *J. Am. Chem. Soc.* **2003**, *125*, 3568; b) A.-C. Gaillot, B. Lanson, V. A. Drits, *Chem. Mater.* **2005**, *17*, 2959.
- [42] a) Y. Song, N. Iyi, T. Hoshide, T. C. Ozawa, Y. Ebina, R. Ma, S. Yamamoto, N. Miyamoto, T. Sasaki, *Dalton Trans.* **2018**, *47*, 3022; b) H. Fukuoka, T. Isami, S. Yamanaka, *J. Solid State Chem.* **2000**, *151*, 40.
- [43] T. Sasaki, F. Kooli, M. Iida, Y. Michiue, S. Takenouchi, Y. Yajima, F. Izumi, B. C. Chakoumakos, M. Watanabe, *Chem. Mater.* **1998**, *10*, 4123.
- [44] a) H.-N. Kim, S. W. Keller, T. E. Mallouk, J. Schmitt, G. Decher, *Chem. Mater.* **1997**, *9*, 1414; b) A. Clearfield, G. D. Smith, *Inorg. Chem.* **1969**, *8*, 431.
- [45] a) A. M. Mathieson, G. F. Walker, *Amer. Mineral.* **1954**, *39*, 231; b) J. McCarney, M. V. Smalley, *Clay Miner.* **1995**, *30*, 187.
- [46] a) D. Yamaguchi, N. Miyamoto, S. Koizumi, T. Nakato, T. Hashimoto, *J. Appl. Crystallogr.* **2007**, *40*, s101; b) M. Gasperin, M. T. Le Bihan, *J. Solid State Chem.* **1982**, *43*, 346.
- [47] W. J. Roth, T. Sasaki, K. Wolski, Y. Song, D.-M. Tang, Y. Ebina, R. Ma, J. Grzybek, K. Kalfurska, B. Gil, M. Mazur, S. Zapotoczny, J. Cejka, *Sci. Adv.* **2020**, *6*, eaay8163.
- [48] M. Swain, *J. Chem. Inf. Model.* **2012**, *52*, 613.
- [49] a) T. Selvam, A. Inayat, W. Schwieger, *Dalton Trans.* **2014**, *43*, 10365; b) S. Vortmann, J. Rius, S. Siegmann, H. Gies, *J. Phys. Chem. B* **1997**, *101*, 1292.
- [50] M. Stöter, S. Rosenfeldt, J. Breu, *Annu. Rev. Mater. Res.* **2015**, *45*, 129.
- [51] a) L. Mayr, S. Amschler, A. Edenharter, V. Dudko, R. Kunz, S. Rosenfeldt, J. Breu, *Langmuir* **2020**, *36*, 3814; b) R. Kunz, S. Amschler, A. Edenharter, L. Mayr, S. Herlitz, S. Rosenfeldt, J. Breu, *Clays Clay Miner.* **2019**, *67*, 481; c) V. Dudko, S. Rosenfeldt, R. Siegel, J. Senker, M. Matejdes, J. Breu, *Langmuir* **2022**, 2022.
- [52] T. Sasaki, M. Watanabe, *J. Phys. Chem. B* **1997**, *101*, 10159.
- [53] a) P. Davidson, C. Penisson, D. Constantin, J.-C. P. Gabriel, *Proc. Natl. Acad. Sci. USA* **2018**, *115*, 6662; b) J.-C. P. Gabriel, F. Camerel, B. J. Lemaire, H. Desvaux, P. Davidson, P. Batail, *Nature* **2001**, *413*, 504.
- [54] R. Liu, T. Gong, K. Zhang, C. Lee, *Sci. Rep.* **2017**, *7*, 9761.
- [55] a) W. J. Roth, T. Sasaki, K. Wolski, Y. Ebina, D.-M. Tang, Y. Michiue, N. Sakai, R. Ma, O. Cretu, J. Kikkawa, K. Kimoto, K. Kalfurska, B. Gil, M. Mazur, S. Zapotoczny, J. Cejka, J. Grzybek, A. Kowalczyk, *J. Am. Chem. Soc.* **2021**, *143*, 11052; b) W. J. Roth, T. Sasaki, K. Wolski, Y. Song, D.-M. Tang, Y. Ebina, R. Ma, J. Grzybek, K. Kalfurska, B. Gil, M. Mazur, S. Zapotoczny, J. Cejka, *Sci. Adv.* **2020**.
- [56] L. J. Michot, I. Bihannic, S. Maddi, S. S. Funari, C. Baravian, P. Levitz, P. Davidson, *Proc. Natl. Acad. Sci. USA* **2006**, *103*, 16101.
- [57] A. Lurf, R. Schoellhorn, *Inorg. Chem.* **1977**, *16*, 2950.
- [58] a) M. M. J. Treacy, S. B. Rice, A. J. Jacobson, J. T. Lewandowski, *Chem. Mater.* **1990**, *2*, 279; b) K. Domen, Y. Ebina, S. Ikeda, A. Tanaka, J. N. Kondo, K. Maruya, *Catal. Today* **1996**, *28*, 167; c) R. E. Schaak, T. E. Mallouk, *Chem. Mater.* **2000**, *12*, 3427; d) Y. Song, N. Iyi, T. Hoshide, T. C. Ozawa, Y. Ebina, R. Ma, N. Miyamoto, T. Sasaki, *Chem. Commun.* **2015**, *51*, 17068.
- [59] R. Ma, Z. Liu, K. Takada, N. Iyi, Y. Bando, T. Sasaki, *J. Am. Chem. Soc.* **2007**, *129*, 5257.
- [60] E. Paineau, I. Bihannic, C. Baravian, A.-M. Philippe, P. Davidson, P. Levitz, S. S. Funari, C. Rochas, L. J. Michot, *Langmuir* **2011**, *27*, 5562.
- [61] R. Mizuguchi, H. Imai, Y. Oaki, *Nanoscale Adv.* **2020**, *2*, 1168.
- [62] a) Q. L. Zhu, C. F. Dai, D. Wagner, O. Khoruzhenko, W. Hong, J. Breu, Q. Zheng, Z. L. Wu, *Adv. Sci.* **2021**, *8*, 2102353; b) Q. L. Zhu, C. Du, Y. Dai, M. Daab, M. Matejdes, J. Breu, W. Hong, Q. Zheng, Z. L. Wu, *Nat. Commun.* **2020**, *11*, 5166; c) Q. L. Zhu, C. F. Dai, D. Wagner, M. Daab, W. Hong, J. Breu, Q. Zheng, Z. L. Wu, *Adv. Mater.* **2020**, *32*, 2005567.
- [63] a) O. Khoruzhenko, D. R. Wagner, S. Mangelsen, M. Dulle, S. Förster, S. Rosenfeldt, V. Dudko, K. Ottermann, G. Papastavrou, W. Bensch, J. Breu, *J. Mater. Chem. C* **2021**, *9*, 12732; b) K. Sano, Y. S. Kim, Y. Ishida, Y. Ebina, T. Sasaki, T. Hikima, T. Aida, *Nat. Commun.* **2016**, *7*, 12559.
- [64] M. Röhr, J. H. Mettke, S. Rosenfeldt, H. Schmalz, U. Mansfeld, R. L. Timmins, C. Habel, J. Breu, F. Durst, *J. Coat. Technol. Res.* **2021**, *19*, 487.
- [65] J. Lange, Y. Wyser, *Packag. Technol. Sci.* **2003**, *16*, 149.
- [66] a) A. G. Erlat, R. J. Spontak, R. P. Clarke, T. C. Robinson, P. D. Haaland, Y. Tropsha, N. G. Harvey, E. A. Vogler, *J. Phys. Chem. B* **1999**, *103*, 6047; b) Y. Letierrier, *Prog. Mater. Sci.* **2003**, *48*, 1.
- [67] a) E. L. Cussler, S. E. Hughes, W. J. Ward, R. Aris, *J. Membr. Sci.* **1988**, *38*, 161; b) T.-Y. Tsai, C.-H. Li, C.-H. Chang, W.-H. Cheng, C.-L. Hwang, R.-J. Wu, *Adv. Mater.* **2005**, *17*, 1769.
- [68] M. Schlenk, E. Hofmann, S. Seibt, S. Rosenfeldt, L. Schrack, M. Drechsler, A. Rothkirch, W. Ohm, J. Breu, S. Gekle, S. Förster, *Langmuir* **2018**, *34*, 4843.
- [69] a) E. S. Tsurko, P. Feicht, F. Nehm, K. Ament, S. Rosenfeldt, I. Pietsch, K. Roschmann, H. Kalo, J. Breu, *Macromolecules* **2017**, *50*, 4344; b) D. A. Kunz, J. Schmid, P. Feicht, J. Erath, A. Fery, J. Breu, *ACS Nano* **2013**, *7*, 4275; c) R. L. Timmins, A. Kumar, M. Röhr, K. Havlíček, S. Agarwal, J. Breu, *Macromol. Mater. Eng.* **2022**, *307*, 2100727.
- [70] M. Röhr, L. K. S. Federer, R. L. Timmins, S. Rosenfeldt, T. Dörres, C. Habel, J. Breu, *ACS Appl. Mater. Interfaces* **2021**, *13*, 48101.
- [71] M. W. Möller, D. A. Kunz, T. Lunkenbein, S. Sommer, A. Nennemann, J. Breu, *Adv. Mater.* **2012**, *24*, 2142.
- [72] C. Habel, M. Schöttle, M. Daab, N. J. Eichstaedt, D. Wagner, H. Bakhshi, S. Agarwal, M. A. Horn, J. Breu, *Macromol. Mater. Eng.* **2018**, *303*, 1800333.
- [73] E. S. Tsurko, P. Feicht, C. Habel, T. Schilling, M. Daab, S. Rosenfeldt, J. Breu, *J. Membr. Sci.* **2017**, *540*, 212.
- [74] C. Habel, E. S. Tsurko, R. L. Timmins, J. Hutschreuther, R. Kunz, D. D. Schuchardt, S. Rosenfeldt, V. Altstädt, J. Breu, *ACS Nano* **2020**, *14*, 7018.
- [75] L. Nurdijayanto, H. Nishijima, Y. Miyake, N. Sakai, M. Osada, T. Sasaki, T. Taniguchi, *Nano Lett.* **2021**, *21*, 7044.
- [76] L. Liu, Z.-L. Yu, J. Qu, J. Huang, *Mater. Chem. Front.* **2021**, *5*, 4658.

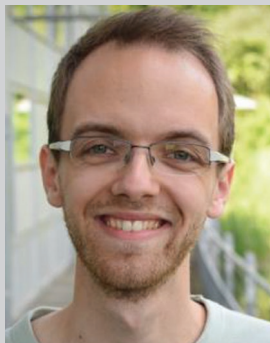
- [77] E. M. Ahmed, *J. Adv. Res.* **2015**, *6*, 105.
- [78] K. Y. Lee, D. J. Mooney, *Chem. Rev.* **2001**, *101*, 1869.
- [79] a) K. Haraguchi, T. Takehisa, *Adv. Mater.* **2002**, *14*, 1120; b) F. Song, X. Li, Q. Wang, L. Liao, C. Zhang, *J. Biomed. Nanotechnol.* **2015**, *11*, 40.
- [80] K. Sano, Y. Ishida, T. Aida, *Angew. Chem., Int. Ed.* **2018**, *57*, 2532.
- [81] M. Liu, Y. Ishida, Y. Ebina, T. Sasaki, T. Hikima, M. Takata, T. Aida, *Nature* **2015**, *517*, 68.
- [82] K. Sano, Y. O. Arzoo, Y. Ishida, Y. Ebina, M. Osada, T. Sasaki, T. Hikima, T. Aida, *Angew. Chem., Int. Ed.* **2018**, *57*, 12508.
- [83] Z. Sun, Y. Yamauchi, F. Araoka, Y. S. Kim, J. Bergueiro, Y. Ishida, Y. Ebina, T. Sasaki, T. Hikima, T. Aida, *Angew. Chem., Int. Ed.* **2018**, *57*, 15772.
- [84] Y. S. Kim, M. Liu, Y. Ishida, Y. Ebina, M. Osada, T. Sasaki, T. Hikima, M. Takata, T. Aida, *Nat. Mater.* **2015**, *14*, 1002.
- [85] R. Ma, X. Liu, J. Liang, Y. Bando, T. Sasaki, *Adv. Mater.* **2014**, *26*, 4173.
- [86] P. M. Saengdet, M. Ogawa, *Chem. Commun.* **2022**, *58*, 3278.
- [87] M. Stöter, B. Biersack, S. Rosenfeldt, M. J. Leidl, H. Kalo, R. Schobert, H. Yersin, G. A. Ozin, S. Förster, J. Breu, *Angew. Chem., Int. Ed.* **2015**, *54*, 4963.
- [88] M. Matejdes, M. Stöter, R. Czerwieńiec, M. Leidl, S. Rosenfeldt, T. Schumacher, J. Albert, M. Lippitz, H. Yersin, J. Breu, *Adv. Opt. Mater.* **2021**, *9*, 2100516.
- [89] P. Ganter, B. V. Lotsch, *Mol. Syst. Des. Eng.* **2019**, *4*, 566.
- [90] E. Mouri, C. Ogami, T. Fukumoto, T. Nakato, *Chem. Lett.* **2020**, *49*, 717.
- [91] a) P. H. Michels-Brito, V. Dudko, D. Wagner, P. Markus, G. Papastavrou, L. Michels, J. Breu, J. O. Fossum, *Sci. Adv.* **2022**, *8*, eabl8147; b) N. Miyamoto, S. Yamamoto, *ACS Omega* **2022**, *7*, 6070.
- [92] K. El Rifaii, H. H. Wensink, C. Goldmann, L. Michot, J.-C. P. Gabriel, P. Davidson, *Soft Matter* **2021**, *17*, 9280.
- [93] W. Yang, S. Yamamoto, K. Sueyoshi, T. Inadomi, R. Kato, N. Miyamoto, *Angew. Chem.* **2021**, *133*, 8547.
- [94] K. Sano, X. Wang, Z. Sun, S. Aya, F. Araoka, Y. Ebina, T. Sasaki, Y. Ishida, T. Aida, *Nat. Commun.* **2021**, *12*, 6771.
- [95] a) P. Sun, R. Ma, X. Bai, K. Wang, H. Zhu, T. Sasaki, *Sci. Adv.* **2017**, *3*, e1602629; b) A. C. Neto, F. Guinea, N. M. Peres, K. S. Novoselov, A. K. Geim, *Rev. Mod. Phys.* **2009**, *81*, 109; c) V. Tran, R. Soklaski, Y. Liang, L. Yang, *Phys. Rev. B* **2014**, *89*, 235319.
- [96] J.-J. Shao, K. Raidongia, A. R. Koltonow, J. Huang, *Nat. Commun.* **2015**, *6*, 7602.
- [97] a) A. van den Berg, H. G. Craighead, P. Yang, *Chem. Soc. Rev.* **2010**, *39*, 899; b) K. Raidongia, J. Huang, *J. Am. Chem. Soc.* **2012**, *134*, 16528.
- [98] P. Sun, R. Ma, T. Sasaki, *Chem. Sci.* **2018**, *9*, 33.
- [99] a) A.-K. Hatz, I. Moudrakovski, S. Bette, M. W. Terban, M. Etter, M. Joos, N. M. Vargas-Barbosa, R. E. Dinnebier, B. V. Lotsch, *Chem. Mater.* **2021**, *33*, 7337; b) M. Tian, L. Wang, J. Wang, S. Zheng, F. Wang, N. Shao, L. Wang, *ACS Sustainable Chem. Eng.* **2022**, *10*, 1137; c) J. Lao, R. Lv, J. Gao, A. Wang, J. Wu, J. Luo, *ACS Nano* **2018**, *12*, 12464.
- [100] T. Zhang, H. Bai, Y. Zhao, B. Ren, T. Wen, L. Chen, S. Song, S. Komarneni, *ACS Nano* **2022**, *16*, 4930.
- [101] a) S. Qin, D. Liu, G. Wang, D. Portehault, C. J. Garvey, Y. Gogotsi, W. Lei, Y. Chen, *J. Am. Chem. Soc.* **2017**, *139*, 6314; b) C. Wei, A. J. Bard, S. W. Feldberg, *Anal. Chem.* **1997**, *69*, 4627.



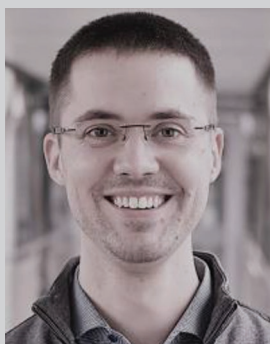
Volodymyr Dudko is currently a Ph.D. candidate working under the supervision of Prof. Josef Breu at the University of Bayreuth. He received his master's degree in Material science and physical chemistry from Erasmus Mundus SERP+ 2019. His current research interests are the delamination of 2D materials.



Olena Khoruzhenko is currently a Ph.D. candidate working under the supervision of Prof. Josef Breu at the University of Bayreuth. She received her master's degree in chemical engineering from Igor Sikorsky Kyiv Polytechnic Institute in 2019. Her current research interests are the functional liquid crystals.



Sebastian Weiß is currently a Ph.D. candidate working under the supervision of Prof. Josef Breu at the Bavarian Center for Battery Technology at the University of Bayreuth. He received his master's degree in Material Chemistry and Catalysis at the University of Bayreuth in 2019. His current research interests are the development and modification of battery cathodes.



Matthias Daab is currently coordinator at the Bavarian Center for Battery Technology (BayBatt). He studied Chemistry at the University of Bayreuth, where he obtained his doctoral degree in Inorganic Chemistry on quantitative delamination in 2018. Before he took up his current job at BayBatt, he was active in the field of industrial formulation chemistry.



Patrick Loch performed his Ph.D. research in the group of Josef Breu at the chair of Inorganic Chemistry I at the University of Bayreuth. Prior, he received his B.Sc. in Chemistry and his M.Sc. in Materials Chemistry and Catalysis from the University of Bayreuth. His main research interests cover the synthesis of functional layered materials, their characterization and application.



Wilhelm Schwieger studied chemistry at the Martin Luther University Halle-Wittenberg (Germany), where he received his Ph.D. degree in chemistry in 1979. In 1998, he became full professor at the Institute of Chemical Reaction Engineering in the Department of Chemical and Biological Engineering (CBI) at the Friedrich-Alexander-Universität Erlangen-Nürnberg (FAU). His main research interests cover the development of new synthesis routes for zeolites and hierarchically porous materials, bifunctional core-shell catalysts and layered materials, structure-activity relationships of catalyst and adsorbents, as well as application-driven development of novel structured reactor concepts.



Josef Breu is full professor in the Department of Chemistry, a member of the Bavarian Polymer Institute, and the Bavarian Center for Battery Technology at University of Bayreuth. Before joining the University of Bayreuth in 2003, he was a postdoctoral fellow at the Royal Institution of Great Britain and assistant professor at the University of Regensburg. His lab is focused on 2D materials, microporous organically pillared silicates (MOPS), high barrier nanocomposites, and meso-structuring of inorganic colloids.